TAp73 is a marker of glutamine addiction in medulloblastoma

Maria Victoria Niklison-Chirou[1*], Ida Erngren[2], Mikael Engskog[2], Jakob Haglöf[2], Daniel Picard[3,4], Marc Remke[3,4], Phelim Hugh Redmond McPolin[1], Matthew Selby[5], Daniel Williamson[5], Steven C. Clifford[5], David Michod[6], Michalis Hadjiandreou[1], Torbjörn Arvidsson[2,7], Curt Pettersson[2], Gerry Melino[8] and Silvia Marino[1]

1-Blizard Institute, Barts and the London School of Medicine and Dentistry, Queen Mary University of London, 4 Newark Street, London, E1 2AT, UK

2-Department of Medicinal Chemistry, Analytical Pharmaceutical Chemistry, Uppsala University, 751 23 Uppsala, Sweden

3-Department of Pediatric Oncology, Hematology and Clinical Immunology, and Department of Neuropathology, Medical Faculty, Heinrich Heine University Dusseldorf, 40225 Dusseldorf, Germany

4 Department of Pediatric Neuro-Oncogenomics, German Cancer Consortium (DKTK) and German Cancer Research Center (DKFZ), 69120 Heidelberg, Germany

5- Wolfson Childhood Cancer Research Centre, Northern Institute for Cancer Research, Newcastle University, NE1 7RU, Newcastle upon Tyne, UK

6-University College of London, Institute of Child Health, WC1N 1EH, London, UK

7-Medical Product Agency, Dag Hammarskjölds väg 42, SE-751 03 Uppsala, Sweden

8-Medical Research Council, Toxicology Unit, Leicester University, Lancaster Road, Leicester LE1 9HN, UK.

Running title: p73 regulates GLS-2 in medulloblastoma

Keywords: medulloblastoma, p73, glutamine, metabolomics

***Corresponding author**

Maria Victoria Niklison-Chirou

Blizard Institute

4 Newark Street

London E1 2AT

m.niklison-chirou@qmul.ac.uk

Tel +44 207 882 2360

Fax +44 207 882 2180

Abstract

Medulloblastoma is the most common solid primary brain tumor in children. Remarkable advancements in the understanding of the genetic and epigenetic basis of these tumors have informed their recent molecular classification. However, the genotype/phenotype correlation of the subgroups remains largely uncharacterised. In particular, the metabolic phenotype is of great interest because of its druggability which could lead to the development of novel and more tailored therapies for a subset of medulloblastoma.

p73 plays a critical role in a range of cellular metabolic processes. We show overexpression of p73 in a proportion of non-WNT medulloblastoma. In these tumors, p73 sustains cell growth and proliferation via regulation of glutamine metabolism. We validate our results in a xenograft model in which we observe an increase in survival time in mice on glutamine restriction diet. Notably, glutamine starvation has a synergistic effect with cisplatin, a component of the current medulloblastoma chemotherapy. These findings raise the possibility that glutamine depletion can be used as an adjuvant treatment for p73-expressing medulloblastoma.

Introduction

Medulloblastoma (MB) is the most common primary paediatric brain tumor and it is a major cause of mortality and morbidity in paediatric oncology (Louis et al. 2007). Current treatment strategies include a combination of surgery, radiotherapy and chemotherapy; they have achieved 70-80% 5-year survival rates, however recurrence is common and it often proves fatal (Hill et al. 2015). In addition, both the brain exposure to ionising radiation and the systemic exposure to chemotherapy agents can induce severe side effects leading to mental and physical disability of the affected children.

MB is a heterogeneous tumor with molecularly defined subgroups which arise from different cerebellar progenitor cells, albeit often showing rather similar histological features (Corno et al. 2012). MB have recently been classified into four molecular groups namely: WNT Group, Sonic Hedgehog (SHH) Group, Group 3 (G3) and Group 4 (G4) (Taylor et al. 2012). The discovery that mutant TP53 plays an important role in SHH MB pathogenesis led to the further dissection of the SHH group into a TP53 wild-type and TP53 mutant subgroups, the latter being associated with a poor outcome (Ramaswamy et al. 2015). Emerging evidence suggests that each group may require specific therapeutic strategies (Northcott et al. 2012) and recent papers demonstrated that WNT MB had anomalous vascularization and show increased haemorrhaging (Phoenix et al. 2016).

The p53-family comprises three members: p53, p63 and p73 (Boominathan 2010) and its role in promoting cell death and senescence has been extensively described. Importantly, p63 plays a particular role in the development of the epidermis (Vanbokhoven et al. 2011) and p73 is essential for the development of the central nervous system (CNS) (Yang et al. 2000). Indeed, p73 is highly expressed in the hippocampus, cortex and cerebellum during embryonic stages of CNS development; its expression then decreases after birth and it is restricted to the neural stem cell (NSC) niches in the adult brain (Pozniak et al. 2002). p73-deficient mice show prominent brain malformations and reduced NSC proliferation (Talos et al. 2010). Unlike p53, p73 is not lost but rather frequently overexpressed in cancer. Accordingly, p73 is overexpressed in MB tumors and cell lines, even though its role in these tumors is still unclear (Zitterbart et al., 2007).

At the molecular level, p73 is transcribed from two different promoters into proteins that either retain (TAp73) or lack (ΔNp73) the transactivation domain. TAp73 is able to activate p53-responsive genes

and induce apoptosis (Zhu et al. 1998), although TAp73 also has distinct transcriptional targets (Allocati et al. 2012). In contrast, ΔNp73 displays anti-apoptotic effect (Dulloo et al. 2010). Recent studies have shown that p73 plays an important role in the regulation of metabolic pathways. TAp73 enhances the pentose phosphate pathway flux (Jiang et al. 2013), activates serine biosynthesis (Amelio et al. 2014b) and controls glutaminolysis (Velletri et al. 2013). TAp73 regulates the mitochondrial respiration by inducting cytochrome *c* oxidase (Rufini et al. 2012) and its depletion results in decreased oxygen consumption and ATP levels, with increased reactive oxygen species (ROS) levels. p73 is also a major transcriptional regulator of autophagy (He et al. 2013) and is activated when mTOR is inhibited (Rosenbluth and Pietenpol 2009). Consistent with these data, TAp73 knockout mice show premature aging and senescence (Rufini et al. 2012).

Metabolic adaptation has recently emerged as a hallmark of cancer and as a promising therapeutic target (Hanahan and Weinberg 2011). Accordingly, highly proliferating cancer cells must adapt their metabolism in order to produce enough energy and mass to replicate. The first step of adaptation is through enhanced aerobic glycolysis, which allows cells to metabolise glucose to lactate instead of pyruvate (Warburg 1956). Aerobic glycolysis in cancer cells is essential for tumor progression and, in MB, has been estimated to account for 60% of ATP production (Moreno-Sanchez et al. 2009).

In addition to the dependency on aerobic glycolysis, cancer cells exhibit other metabolic characteristics such as increased fatty acid synthesis and addiction to glutamine. Some cancer cells show glutamine addiction regardless of the fact that glutamine is a nonessential amino acid and one that can be synthesized from glucose (DeBerardinis and Cheng 2010). Glutamine is used by the cancer cells to synthetize amino acid precursors and in maintaining activation of TOR kinase (Ahluwalia et al. 1990). Moreover, glutamine is the primary mitochondrial substrate, is required to maintain mitochondrial membrane potential and to support the NADPH production needed for redox control and macromolecular synthesis (Wise and Thompson 2010). Importantly, MB metabolism exhibits a high dependency on aerobic glycolysis and lipogenesis through the activation of hexokinase 2 and fatty acid synthase (Gershon et al. 2013; Tech et al. 2015). Additionally, MB limit protein translation through activation of eukaryotic elongation factor 2 kinase, to restrict energy expenditure

(Leprivier et al. 2013). This difference between cancer and normal cells, suggests that targeting metabolic dependence could be a selective approach to treat cancer patients.

In this study, we set out to investigate the metabolic pathways regulated by p73 in MB by means of genome wide transcriptome and metabolome analysis in MB cell lines and patient-derived MB cells with subsequent biochemical and functional validation *in vitro* and *in vivo* in a xenograft mouse model.

Results

TAp73 is overexpressed in MB and controls proliferation in MB cell lines and patient-derived primary cells

p73 was reported to be overexpressed in MB (Zitterbart et al. 2007), although it was unclear which p73 isoforms were expressed. To clarify this, we analysed RNA-sequence data derived from 240 clinically-characterised human MB. Significant overexpression of TAp73α was found in G4 and G3 MB as compared to normal cerebellum with high expression levels found in SHH MB and very low levels in WNT MB (Figure 1A). TAp73β, ΔNp73α and ΔNp73β isoforms were not significantly expressed in MB (Supplemental Fig. S1A). Next, we looked at the expression of p75NTR and GLS-2, two-well characterized TAp73 target genes, important for brain development and glutamine metabolism respectively (Niklison-Chirou et al. 2013; Velletri et al. 2013). Consistently with the TAp73 levels, significant up-regulation of GLS-2 was found in the G4 MB, whilst highest expression of p75NTR was detected in SHH MB (Figure 1A). Overall, these analyses demonstrate that the most aggressive subgroups of MB express high levels of TAp73 mRNA.

Next, we analysed the expression of p73 in a range of human patient-derived primary MB cells and cell lines. We found the highest level in lCb-1299 (primary human G4 MB), intermediate levels in primary SHH MB cells (m137 and m692) and DAOY cell line, with no expression detected in UW228-2 cell line (Supplemental Fig. S1B). We show at the RNA and protein levels that the only isoform expressed in MB cells is TAp73, as a single band of 75kDa was detected in the western blot (Supplemental Fig. S1B, C). RT-PCR analysis of TAp73, p75NTR and GLS-2 in lCb-1299, m137,

m692, DAOY and UW228-2 cells revealed upregulation of all genes in MB cell expressing p73 (Supplemental Fig. S1D-F), in keeping with the results of the genome-wide analysis on human primary tumors (Figure 1A).

To explore the role of TAp73 in MB, we transiently knocked-down p73 (p73KD) in DAOY, m137 and ICb-1299 cells. Western blot and RT-PCR confirmed p73KD in all cells (Supplemental Fig. S1G-H) and showed that the levels of the other p53-family members (p53 or p63) were not affected (Supplemental Fig. S1G). Silencing p73 strongly reduced cell growth in DAOY, m137 and ICb-1299 (Figure 1B). Importantly, we observed a 30% reduction in cell proliferation in ICb-1299 cells, where only a partial (44% of p73 levels) knockdown could be obtained (Figure 1C-D).

These results show that p73 is essential for MB cell growth and proliferation.

TAp73 regulates GLS-2 in MB cells

p73 regulates the expression of many target genes involved in cell metabolism, DNA repair or apoptosis. To dissect the molecular pathways mediating p73's role in MB, we performed a differential gene expression analysis in DAOY comparing p73KD cells with control cells at 48h after silencing. RNAseq analysis revealed that a large number of genes involved in metabolism and/or stress pathways were differentially expressed upon p73KD and unsupervised hierarchical clustering (HCL) demonstrated that DAOY p73KD cluster apart from control cells, suggesting that a distinct transcriptome-wide gene signature was associated with the silencing of p73 (Figure 1E, genes involved in metabolism and Supplemental Fig. S1I, genes involved in stress pathways). Because we were interested in identifying genes that are specifically transactivated by p73, we focussed our attention on genes that are down-regulated in the absence of p73.

We selected 14 genes (>1.5 fold change, $P < 0.05$) for validation as p73 target genes: GADD45B, GLS-2, ASL, SFN, PFKM, ACO2, NOS2, PhKA1, NBN, ENO, AKT2, SDHA, CS and RAD50 (Figure 1E and Supplemental Fig. S1I,J). p73KD was repeated in DAOY cells and expression of the target genes were analysed at three different time points 10, 24 and 48h after silencing. We detected an early down-regulation (10h after knocked-down) of GADD45B, GLS-2 and ASL (Figure 1F and Supplemental Fig. S1K). To assess whether this molecular convergence was retained in patient-

derived primary MB cells expressing p73, the expression of GADD45B, GLS-2 and ASL was assessed in lCb-1299 and m137 after p73KD. In agreement with our previous results, we observed an early down-regulation of GLS-2 in both cell lines upon p73KD (Figure 1F). GADD45B and ASL were only down-regulated in lCb-1299. Importantly, re-expression of a mouse TAp73 rescued the effect of p73KD on the expression levels of GADD45B, GLS-2 and ASL, confirming that they were primary p73 targets in DAOY cells (Figure 1G). Down-regulation of GLS-2 after p73KD was confirmed at the protein level in DAOY cells (Figure 1H).

These results show that GLS-2 is a conserved TAp73 target gene in MB cells derived from non-WNT MB subgroups.

TAp73 is a critical cellular component for mitochondrial bioenergetics in MB cells

The importance of glutamine as a nutrient in cancer relies on its suitability as a substrate for the mitochondrial TCA cycle (Hensley et al. 2013). Since we observed a strong reduction of GLS-2 after p73KD, we measured the mitochondria oxygen consumption rate (OCR) as an indicator of the mitochondrial function. A functional bioenergetics profile of DAOY p73KD as compared to control cells is shown in Figure 2A. We measured the OCR in response to sequential treatment with oligomycin, FCCP and rotenone/antimycin A. We observed a strong decrease in the basal respiration, ATP production and spare respiratory capacity upon p73KD, which suggested a profound respiratory defects after p73KD (Figure 2A). Similar results were obtain after GLS-2KD (Figure 2A and Supplemental Fig. S2A). These findings were validated in patient-derived primary MB cells, m137 and ICb-1299, where similar results were obtained (Supplemental Fig. S2B-C).

Next, we performed a stable p73 knockdown (p73sKD) with two different shRNA p73sKD*3 and p73sKD*5. The reduction of p73 protein levels in steady state was confirmed by immunoblotting (Supplemental Fig. S2D). Importantly, re-expression of GLS-2 in a stable p73 knockdown setting (p73sKD*5) rescued the OCR levels (Supplemental Fig. S2E, F, G).

While assessing whether p73KD induces mitochondrial dysfunction, we observed a strong mitochondrial hyperpolarization in DAOY cells upon p73KD (Supplemental Fig. S2H). Because mitochondrial hyperpolarization has been related to ROS production (Giovannini et al. 2002) and

glutamine is a precursor of glutathione synthesis (GSH, the major antioxidant within the cells), we measured the redox status of DAOY cells upon p73KD or in our stable p73sKD*3, p73sKD*5 or after GLS-2KD as assessed by the GSH/GSSG ratio (Figure 2B). A decreased ratio of reduced glutathione to glutathione disulfide was observed after p73KD or p73sKD or after siGLS-2, confirming that after p73 or GLS-2 knockdown DAOY cells are under oxidative stress. Importantly, this effect was completely rescued after GLS-2 overexpression (Figure 2B), indicating that GLS-2 is an important p73 target gene for balancing the redox status of the cells.

Since 60% of ATP production in MB cells is generated by aerobic glycolysis (Moreno-Sanchez et al. 2009), we measured the extracellular acidification rate (ECAR) in DAOY cells upon p73KD (Figure 2C). The results show a robust decline (50%) in lactate production after p73KD compared with control cells in response to oligomycin treatment, suggesting a reduced ability to increase glycolytic flux under conditions of increased ATP demand.

Next, we set out to confirm these results by measuring the kinetic of glucose uptake and lactate production in DAOY upon p73KD at different time points. In control cells the levels of glucose decreased steadily over time with an increased lactate production observed in parallel; whereas an inhibition of glucose uptake and production of lactate was observed after 20h in DAOY p73KD (Figure 2D-E). Importantly, glucose levels increased in DAOY p73KD, indicating that the lack of TAp73 induced gluconeogenesis in the longer term. Gluconeogenesis is a common process in tumor cells, where cells can derive energy from ketone bodies, which are converted to acetyl-CoA and shunted into the TCA cycle.

Because oxidative phosphorylation and aerobic glycolysis are the two main sources of cellular energy, we measured ATP levels in DAOY, m137 and lCb-1299 cells. In line with our previous results, a strong reduction in the ATP levels was observed upon p73KD in DAOY, m137 and ICb-1299 cells (Figure 2F and Supplemental Fig. S2I). Similar results, were observed upon GLS-2KD (Supplemental Fig. S2I).

Taken together these data suggest that p73 is essential for the major energy-producing pathways and for maintenance of the redox balance of the cells through generation of glutathione via regulation of GLS-2.

p73 sustains activation of the mTOR pathway by inhibiting AMPK activation in MB

AMPK plays a role as a master regulator of cellular energy and is activated when cellular ATP levels drop and initiates a cellular reprogram that allows the cell to adapt to the energetic stress (Hardie et al. 2012). We observed a robust activation of AMPK, as assessed by phosphorylation of its direct target acetyl-CoA carboxylase (ACC), in DAOY after p73KD (Figure 2G). An important mediator of the AMPK response is the mTOR pathway, which is inhibited by AMPK (Liu et al. 2012). We show here inhibition of the mTOR pathway as shown by reduced phosphorylation of its downstream target, the protein S6 kinase (S6K) and eukaryotic translation elongation factor 2 (eEF-2), upon p73KD (Figure 2G).

mTOR is a nutrient sensor, whereby glutamine and leucine levels stimulate protein synthesis via signalling through the mTOR complex. Conversely, mTOR inhibition leads to reduction in the rate of the global protein production (Zhao et al. 2015). In order to determine whether p73 supports protein synthesis in DAOY cells, we silenced p73 in DAOY cells and then treated for 1h with puromycin. The incorporation of puromycin in the newly synthesized proteins was assessed with an anti-puromycin antibody. We found reduced protein synthesis of around 50% in DAOY p73KD (Figure 2H and Supplemental Fig. S2J). These data suggest that p73 modulate mTOR activation through reduction in AMPK activity in MB cells.

Profound metabolic changes in MB cells after p73KD

Cellular metabolism is characterized by many parameters including nutrient uptake or metabolite secretion rates (Buescher et al. 2015). We measured amino acid levels in the medium of DAOY p73KD as compared to controls 48h after silencing. We show that the lack of p73 reduces 14 amino acids and increased the levels of 4. Alanine, glutamine and glutamate are the most noticeably reduced amino acids (Figure 3A). Interestingly, the main source of carbon skeletons used for gluconeogenesis are lactate and the amino acids alanine and glutamine, thus these data are in agreement with our previous observation that p73KD induces gluconeogenesis (Figure 2D).

The four amino acids augmented in the medium are serine, glycine, ornithine and proline (Figure 3A). Serine and glycine are biosynthetically linked, and are essential for one carbon metabolism (Amelio

et al. 2014a). Since these amino acids show increased levels in the absence of the p73, it is likely that this represents a compensatory effect not directly linked to p73. We confirmed these results by measuring the kinetic of serine and glycine production (Supplemental Fig. S3A-B), we observed a significant increase in serine/glycine synthesis after 20h of p73KD. Importantly, serine can be used by cancer cells for the de novo synthesis of ATP (Maddocks et al. 2016).

Next, we measured the expression of pyruvate kinase isozymes M2 (PKM2), an enzyme characterized by a low affinity to its substrate phosphoenolpyruvate (PEP) which is almost inactive at physiological PEP concentrations. High RNA level of PKM2 was observed in DAOY cells after 24 and 48h of p73KD (Figure 3B). Importantly, presence of PKM2 will induce accumulation of glycolytic intermediates above pyruvate kinase and, therefore, will increase the synthesis of serine/glycine or the pentose phosphate pathway flux.

Following, we used liquid chromatography hyphenated to high resolution mass spectrometry (LC-HRMS) based untargeted metabolite profiling to study potential differences in the intracellular polar metabolome (endogenous molecules with a molecular weight below 1000 Da) in DAOY p73KD as compared to controls 48h after silencing. A clear difference between the two conditions was found (Figure 3C-D), indicating that silencing of p73 induces a strong difference in the polar metabolites of the cells. The absence of p73 in DAOY cells induces a significant reduction of adenosine, malic acid and choline, as well as several phospholipids. The reduction in adenosine observed is in agreement with the reduction in ATP levels observed after p73KD (Figure 2F and Supplemental Fig. S2I). Importantly, we observed a strong reduction in choline and phospholipids (Figure 3E), both of which can function as an energy source since they can be degraded to produce acetyl-CoA and the reduction in malic acid is in line with our observation that the activity of the TCA cycle was reduced after p73KD.

Importantly, the levels of cytidine, guanine, guanosine, hypoxanthine, inosine, uridine, phenylalanine, indoleacetic acid, N-formyl-L-methionine, 4-phosphopantohenoylcysteine and pyruvic acid were significantly ($p < 0.05$) up-regulated (Figure 3E). We performed a pathway analysis using the web-based software MetaboAnalyst (www.metaboanalyst.ca). We found that several metabolites were related and we observed an up-regulation of purine metabolism. These data are in line with our

observation that after p73KD we have an increase in serine/glycine synthesis, whereby serine can contribute to the purine metabolism by providing one-carbon units (Maddocks et al. 2016).

During gluconeogenesis, lactate and alanine are consumed to produce pyruvate, hence the strong reduction in alanine and the increase levels of pyruvate that we observed in DAOY p73KD. Pyruvate will be oxidized to feed into the gluconeogenic pathway (Supplemental Fig. S3C).

In summary, silencing of p73 in DAOY cells induces a profound metabolic alteration in which the cells try to compensate for the lack of energy due to reduced glutamine metabolism through a compensatory mechanism. Instead, lactate and pyruvate intermediates are utilized to feed into the gluconeogenic pathway. This process will allow the cells to produce large amount of serine/glycine and synthetize intermediates of the purine pathways and nucleosides probably to synthetize ATP de novo.

TAp73 expression is a biomarker of glutamine addiction in MB cells

Glutamine is an abundant and versatile nutrient that participates in energy formation, redox homeostasis and macromolecular synthesis in cancer cells (Altman et al. 2016). These characteristics make glutamine metabolism an appealing target for new clinical strategies. Importantly, some cancers display addiction to glutamine despite the fact that glutamine is a non-essential amino acid (Wise and Thompson 2010).

Nutrient deprivation is a strong stress with dire consequences on cell viability and energy status (Leprivier et al. 2013). Therefore, we investigated whether removal of the amino acid glutamine or serine/glycine or glucose, induced a differential response between medulloblastoma cells expressing p73 and those without p73. Firstly, we measured the impact on cell growth after glucose (Glc starv), glutamine (Gln starv) and serine/glycine (Ser/Gly starv) starvation. Cell number were recorded in DAOY and UW228-2 cultures after 24h under starvation as examples of a p73 expressing and non-p73 expressing line respectively. In DAOY cells, we observed proliferation arrest under glucose starvation, a significant reduction of the cell number under glutamine starvation and no significant effect under serine/glycine starvation (Figure 4A). Likewise, the three-starvation conditions were able to stop cell proliferation of UW228-2 cells (Figure 4A). Because we observe a reduction in cell number

in DAOY cells after glutamine starvation, we hypostatize that this could be due to cell death. To validate this results, we measured cell proliferation of DAOY and UW228-2 cells under the three-starvation conditions. We found that only Gln-starvation induces a robust inhibition of cell proliferation in DAOY cells after 15h treatment as assessed by EdU incorporation (Figure 4B-C).

It was reported that nutrient deprivation induces autophagy (Filomeni et al., 2015), therefore, we measured the levels of LC3-II by FACS analysis in DAOY and UW228-2 cells in control medium and after 24h under glucose, glutamine or serine/glycine starvation. No increase in LC3-II levels was observed (Supplemental Fig. S4A).

Next, we assessed if glucose, glutamine or serine/glycine was essential for ATP production in DAOY and UW228-2 cell lines. Cells were subjected to starvation for 24h followed by measurement of the ATP levels (Figure 4C). We show a 96% reduction in the ATP levels in DAOY cells after Gln-starvation, while no changes were seen in UW228-2, suggesting that the cell line expressing p73 had a glutamine addiction phenotype (Figure 4D).

p73 protein levels are usually maintained low by rapid proteasome degradation, however DNA damage and different stress signals may trigger the stabilization of p73. Therefore, we measured p73 levels in DAOY cells after 18h under the three-starvation condition (Figure 4E). We observed upregulation of p73 only under glutamine starvation. Importantly, Gln-starvation of DAOY cells for 4, 6 and 8h concomitantly with MG132, a proteasome inhibitor that reduces the degradation of ubiquitin-conjugated proteins, induced enhancement of the p73 stabilization (Supplemental Fig. S4B). Since increased levels of p73 can induce apoptosis (Asher et al. 2005), we measured apoptosis with Annexin/PI in DAOY and UW228-2 cells under the different starvation condition. After 36h of starvation only DAOY cells under Gln-starvation show a strong apoptosis response (Figure 4F), while UW228-2 did not show apoptosis under the three-starvation conditions (Supplemental Fig. S4C).

Next, we challenged DAOY, UW228-2 and the primary G4 cells, lCb-1299, with Gln-starvation or Gln-starvation plus MG132. We show a strong synergistic effect in inducing cell death in DAOY and lCb-1299 after Gln-starvation plus MG132, while no effect was observed in UW228-2 cells (Figure 4G).

Subsequent, we analysed the kinetic of glucose uptake and lactate production in DAOY cells in control medium and under glutamine starvation. We observed that glucose levels decreased steadily over time in DAOY cells in control medium, with an increased lactate production observed in parallel; an inhibition of glucose uptake and production of lactate was observed after 20h in DAOY under Gln-starvation (Supplemental Fig. S4D-E). Importantly, we were unable to detect the induction of gluconeogenesis under Gln-starvation condition. Therefore, we measured serine and glycine levels in the medium of DAOY cells in control medium or under Gln-starvation condition (Supplemental Fig. S4F-G). We observed an initial drop in serine and glycine levels, but at a later time point, 40h, the levels were equal to control. These data suggest that under Gln-starvation condition, DAOY cells are not able to induce a metabolic reprogramming to allow them to adapt and survive under glutamine starvation.

These data strongly support our hypothesis that expression of p73 predicts a phenotype of glutamine addiction in MB cells.

Synergistic effect of glutamine starvation and cisplatin in MB cells expressing p73

Cisplatin and etoposide are effective in MB patients (Evans et al. 2009) and, therefore, we treated DAOY cells with glutamine starvation in conjunction with two different concentrations of cisplatin or etoposide for 18h. Importantly, we found a strong enhancement of the apoptotic effect after Gln-starvation plus cisplatin while no effect was seen with the Gln-starvation plus etoposide treatment (Figure 5A).

Next, we evaluated the impact on cell proliferation, as assessed by EdU incorporation in lCb-1299 primary cells treated with Gln-starvation or compound 968 with or without cisplatin for 18h. Compound 968 is a cell-permeable, inhibitor of GLS-2 which mimic a condition of glutamine starvation. We observed that Gln-starvation or compound 968 alone induced 25 or 30% inhibition in cells proliferation respectively (Figure 5B and Supplemental Fig. S5A). Importantly, the combination of Gln-starvation plus cisplatin or compound 968 plus cisplatin induced a strong synergic effect of 45 to 80% inhibition in cell proliferation (Figure 5B and Supplemental Fig. S5A).

To assess whether p73 was mediating the apoptotic response upon Gln-starvation, we performed a stable p73 knockdown (p73sKD*3 and p73sKD*5). A robust apoptosis was observe in DAOY cells after Gln-starvation or Gln-starvation plus cisplatin after 30h of treatment (Figure 5C). Importantly, no effect was observed under Gln-starvation in both p73sKD cells with only negligible apoptosis observed under Gln-starvation plus cisplatin in both p73KD cells. Furthermore, a strong reduction in ATP levels was observed in control DAOY cells after Gln-starvation or Gln-starvation plus cisplatin but the effect was abolished in DAOY p73sKD (Figure 5D). These data support the conclusion that p73 is an important element to mediate apoptosis in MB cells under glutamine starvation.

To confirm the "glutamine addiction phenotype" in MB primary cells, we evaluated the cell number and the ATP levels after treatment with Gln-starvation, cisplatin, Gln-starvation plus cisplatin, 6-Diazo-5-oxo-L-norleucine (DON, a glutamine antagonist) or DON plus cisplatin in m137 and lCb-1299 human primary cells. We demonstrated a synergistic effect resulting in a reduction of cell number only when cells expressing p73 were treated with the combination of Gln-starvation plus cisplatin or DON plus cisplatin (Figure 5E). Instead, a strong reduction of ATP levels is observed already under Gln-starvation or DON treatment (Supplemental Fig. S5B), in keeping with MB cells expressing p73 using glutamine as a primary source of energy.

These results confirm the glutamine addiction phenotype of MB cells expressing p73.

Glutamine starvation induces ROS and DNA damage in MB cells expressing p73

Nutrient deprivation induce reactive oxygen species (ROS) (Wu et al. 2013) and, therefore, we asked if glucose, glutamine or serine/glycine starvation could induce the accumulation of ROS with subsequent induction of DNA damage. We starved DAOY and UW228-2 cells of glucose, glutamine or serine/glycine for 12h, followed by ROS assessment with the probe H_2DCFDA. We observed that under the three starvation condition, DAOY and UW228-2 cells underwent a redox imbalance reflected by increased ROS levels (Figure 6A), an effect that was prevented by the addition of N-acetyl cysteine (NAC) (Figure 6B and Supplemental Fig. S6A).

We next assessed whether the increased ROS levels induced DNA damage. DNA double strand breaks (DSBs) were visualized by immunostaining for phospho-serine 139 histone 2AX (γ-H_2AX) as

nuclear foci at the sites of damage in DAOY cell nuclei 24h post starvation. Confocal imaging of γ-H_2AX foci indicated that Gln-starvation induced foci that were more abundant and significantly larger in DAOY cells as compared to control cells (Figure 6C-D). Similar findings were not observed after glucose or serine/glycine starvation treatment. Furthermore, the combination Gln-starvation plus cisplatin induced an accumulation of foci in the nuclei at 10h that were comparable to Gln-starvation alone after 24h. This results suggest that cisplatin treatment induce a synergistic effect with Gln-starvation.

Next, we measured the redox status with GSH/GSSG ratio, as a marker for oxidative stress, in DAOY and UW228-2 cells in control medium and in glucose, glutamine or serine/glycine starvation. We found that the levels of GSH/GSSH ratio dropped significantly in DAOY cells under Gln-starvation, less so under serine/glycine starvation and not significantly under glucose starvation (Figure 6E). Importantly, no effect in GSH/GSSH ratio was observed in UW228-2 cells.

To confirm this result, we measured NADH levels in these cells under the different starvation conditions, because NADH levels are a well-recognized indicator for cellular metabolic homoeostasis. In fact, increased ROS level and reduced NADH levels represent a status of metabolic imbalance (Li et al. 2016). We show a significant reduction of the NADH levels under Gln-starvation in DAOY cells, while no effect was observed in UW228-2 cells (Figure 6F).

Together these results suggest that MB cells that express p73 show a glutamine addiction phenotype, at least in part by maintaining an oxidant detoxification capacity.

Glutamine restriction diet reduce medulloblastoma tumor growth

We then set out to validate our *in vitro* results in an *in vivo* mouse model of medulloblastoma. Firstly, we show that chronic depletion of non-essential amino acid glutamine (glutamine restriction diet) is well tolerated *in vivo* (Supplemental Fig. S7A). Subsequently, ion-exchange chromatography confirmed a significant drop in the levels of glutamine and glutamate, but not other amino acids, in the cerebellum and in the cerebrospinal fluid (CSF) of mice treated with glutamine restriction diet (Figure 7A-B and Supplemental Fig. S7B-D). Importantly, high levels of serine were observed in normal cerebellar tissue after Gln-restriction diet (Figure 7A), suggesting that normal cells could use serine

metabolism for de novo ATP synthesis and survive under Gln-restriction diet. Injection of ICb-1299 in the cerebellum of new-born NOD-SCID mice rapidly induced tumors with histological and immunohistochemical features of MB (Supplemental Fig. S7E). Animals fed with a Gln-restriction diet displayed a significant increase in survival time compared to those mice fed a control diet (Figure 7C). Importantly, the combination of Gln-restriction diet with cisplatin (2 and 3 doses) induced a significant synergic effect and extended the survival time (Figure 7C). Indeed, we detected a significant reduction in cell proliferation (Ki67 staining) with a strong increase in apoptosis (cleaved caspase-3) in the animals fed with Gln-restriction diet while being treated with cisplatin as compared to control mice (Figure 7D).

These results are in agreement with our *in vitro* data where Gln-starvation leads to reduced proliferation and increased apoptosis in synergism with cisplatin in MB cells expressing p73.

Discussion

Medulloblastoma represent a heterogeneous group of brain tumors with distinct molecular and pathological features. Current treatments for MB include surgery, radio- and chemotherapy, which induce severe side effects in a substantial proportion of patients. We have focused on elucidating the metabolic vulnerabilities of MB for the development of a new therapeutic strategy to minimize the adverse effects of the current therapy.

We show here that TAp73α is over-expressed in a proportion of MB, including aggressive subgroups, a finding which confirms and further extends the original description of p73 protein over-expression in MB (Zitterbart et al. 2007).

Numerous evidence suggest that p73 has a well-defined role in cell metabolism and brain development (Agostini et al. 2016). However, because of the existence of numerous splice variants as well as because of the regulation of protein stability by proteasomal degradation and micro-RNA, its precise effect on cellular metabolism is currently ill defined.

We set out to assess whether p73 regulate any aspect of cell metabolism in human MB and to characterize the relationship between p73 status and the sensitivity to glutamine restriction treatment. Therefore, we silenced p73 in MB cell lines and patient-derived MB cells and we assessed metabolic

changes by genome wide transcriptome and global metabolite profiling. The global metabolite profiling is a novel and powerful approach to gain a comprehensive analysis of small endogenous metabolites (Nicholson et al. 1999). Such data can be used to form a hypothesis describing possible metabolic alternations due to perturbation of the cellular system (Haggblad Sahlberg et al. 2017). Overall, our studies shows for the first time that TAp73 is essential for accurate mitochondrial bioenergetics, at least in part by modulating GLS-2 expression, in agreement with previous data in a non-neoplastic context (Velletri et al. 2013).

The role of GLS-2 in tumorigenesis is context specific and regulated by factors that are still incompletely characterized (Hensley et al. 2013). GLS-2 is a mitochondrial protein that hydrolyse glutamine to glutamate. Following this, glutamate will be used in the cells as a substrate in the TCA cycle or for glutathione synthesis. We show that p73KD-induced growth inhibition in MB and it is directly linked to reduced mitochondria respiration rates and glycolytic capacity. Notably, our data suggest that MB cells expressing p73 may be more dependent on mitochondrial respiration for ATP production. Taken together these data suggest that TAp73 plays an essential role in maintenance of MB cell energy.

Cells regulate energy levels through AMPK, which acts as a sensor of the ATP/ADP ratio (Hardie et al. 2012). AMPK activation induces metabolic changes leading to ATP renewal with inhibition of ATP consumption (Wu et al. 2013). The changes in ATP levels trigger the activation of the energetic stress responses (Mihaylova and Shaw 2011). The function of AMPK is partly mediated by mTOR, which lies at the heart of a nutrient-sensing signalling network that controls cellular metabolism (Liu et al. 2012). After p73KD, we observed a strong activation of AMPK with a robust inhibition of mTOR, suggesting that p73 maintains the activation of mTOR pathway through modulation of AMPK activity.

We demonstrate that p73KD induces a robust reprograming of metabolic process, including *de novo* glucose synthesis, also called gluconeogenesis. This process allows cells to synthetize serine/glycine and pentose phosphate pathway components from glycolytic intermediates. The role of serine in one-carbon metabolism to support the methionine cycle is well documented (Meiser et al. 2016) and recently it was also implicated in *de novo* ATP synthesis (Maddocks et al. 2016). After p73KD, we observed enhanced rates of *de novo* purine synthesis and nucleoside, which may hint at an enhanced

contribution to RNA and DNA synthesis. However, because p73KD induces inhibition of cell proliferation, it is most likely that the cells are using serine/glycine pathway for ATP generation after p73 silencing, as previously demonstrated in colon cancer (Maddocks et al. 2016).

Over the past forty years, it has become increasingly clear that tumor cells exhibit specific amino acid dependency and cells from different tumors were shown to die quickly *in vitro* following arginine, cysteine or glutamine deprivation, whilst normal cells survived (Liu et al. 2015). p53-deficient tumors are vulnerable to serine/glycine starvation (Maddocks et al. 2013) although current therapies do not fully exploit this major difference between cancer cells and non-neoplastic cells.

Here, we demonstrate that MB cells expressing p73 are “glutamine addicted”. Glutamine plays an important role in supporting tumor growth as it is essential for the synthesis of glutathione, an important mitochondrial antioxidant (Amores-Sanchez and Medina 1999). Glutathione is capable of preventing damage of different cellular components caused by ROS such as free radicals, peroxides or lipid peroxides (Mari et al. 2009). MB growth *in vitro* is inhibited in p73-expressing cells under Gln-starvation and it is associated with an abrupt depletion of intracellular ATP. Importantly, MB cells under Gln-starvation show DNA damage, even though all three-starvation conditions induce over production of ROS. A wealth of literature supports the role of p73 in inducing apoptosis after DNA damage (Allocati et al. 2012). We show that only Gln-starvation induces TAp73 stabilization. Indeed, combination of Gln-starvation with cisplatin (a chemotherapy agent of choice in MB therapy) induced a dramatic apoptotic response possibly because of a mitochondria ROS response known to be triggered by cisplatin (Marullo et al. 2013). In keeping with this interpretation, treatment with etoposide did not elicit a similar effect. We validated p73's role in inducing apoptosis following glutamine starvation through the use of a stable p73 knockout. Crucially, these cells became refractory to glutamine starvation. This suggests that any drug inducing p73 stabilization or DNA damage will have a synergistic effect with Gln-starvation.

To validate these results in an *in vivo* mouse model of medulloblastoma, we generated orthotropic xenografts of patient derived MB cells expressing p73 in NOD-SCID mice. Kaplan-Meier analyses showed that Gln-restriction diet induces a significant increase in the overall survival rate of the xenografted mice with a significant reduction in cell proliferation (Ki67) and increase in apoptosis

(cleavage caspase-3). Importantly, we observed a synergic effect between Gln-restriction diet and cisplatin treatment, raising the possibility that glutamine restriction diets could be used as an adjuvant treatment for p73-expressing medulloblastoma.

In summary, we show that p73 support mitochondria respiration in MB via regulation of glutamine metabolism. Importantly, we validate the susceptibility to Gln-restriction diet of p73 expressing MB in a xenograft model. The findings presented here support the notion that p73 is a marker of glutamine addiction in MB tumors and raise the possibility that glutamine restriction diet could be implemented to maximize MB growth control while minimizing treatment toxicity.

Material and Methods

LC-HRMS based metabolite profiling. The analysis was performed using an Acquity UPLC I-class system from Waters (Manchester, UK) coupled to a G2S Synapt Q-TOF equipped with an electro spray ionization (ESI) source (Waters). The sample separation was performed on a HILIC-Amide column (1.7 µm, i.d. 2.1x50 mm) from Waters and the column temperature was kept at 40°C.

Extra-cellular amino acid measurement: The medium and cerebellar extracts were centrifuged and the supernatant was analysed. For CFS, at least 1µL of CFS per animal was extracted. Next, 1µL of CSF was diluted to 500µL with deionized water and analysed. Analysis was performed by ion-exchange chromatography, post column derivitisation with ninhydrin and photometric detection.

Extra-cellular glucose and lactate measurement: Medium from DAOY control and sip73 cells was collected a different time points. The medium was centrifuged and the supernatant was analysed with an Accutrend®Plus System (Roche) according to the manufacturer's instructions.

Measurement of Intracellular ROS: The DAOY and UW228-2 cells were incubated with 5µM C-DCDHF-DA-AM (Invitrogen) for 30min. ROS fluorescence (emission:~530nm) was measured by a 200ms-exposure (excitation:~480 nm).

Xenografts mouse model: All procedures had Home Office approval (Animals Scientific Procedures Act 1986, PPL:70/7275). NOD-SCID were divided randomly into two groups (Control diet or Gln-restriction diet), each group consisting of 10 mice.

Statistical analysis: All results are expressed as mean values ±SD or ±SEM of at least three independent experiments. The unpaired Student's t test and analysis of variance (one-way Anova) was used to assess significant differences between results. P values <0.05 were considered statistically significant.

Author Contributions

MVNC, PHRM and MH conducted the experiments. MVNC, DM, GM and SM designed the experiments and wrote the paper. DP and MR perform the RNAseq analysis. MS, DW and SCC performed the analysis of p73 levels in human MB data set. IE, ME, JM, TA and CP performed the metabolomics analysis.

Acknowledgments

We are grateful to Patrick Pallier, Xinyu Zhang, Thomas Millner, Ashirwad Merve, Anthony Price and Samuel Carney for their helpful advice. Peter Dirks and Xiao-Nan Li for the gift of patient-derived low passages MB cells. This work was funded by Children with Cancer UK fellowship (Reference Nº2014/178) awarded to MVNC, the Medical Research Council UK project grant (MR/N000528/1) to SM and Medical Research Council UK programme grant to GM.

Figure legends

Figure 1. p73 is overexpressed in medulloblastoma and regulates GLS-2 expression. A) Box plot representation of TAp73α, p75NTR and GLS-2 expression levels (FPKM: fragments per kilobase of transcript per million mapped reads) across a cohort of 240 primary MB. Patient number per group are WNT:28, SHH:58, G3:59, G4:95, CB:3 ***P<0.001. B) DAOY, m137 and ICb-1299 cells were transiently transfected with scramble or sip73 (sip73*1: ID: 2671, sip73*2: ID: 115666). After 48h, cells under different treatments were counted in triplicates. For apoptosis assessment (% of cells in SubG1), cells were stained with PI and analysed by FACS. C) Confocal microscope images of ICb-1299 scramble cells or sip73*2 after 48h. We assessed cell proliferation by EdU incorporation. Size bar=20μm. D) Quantification of EdU staining in ICb-1299 scramble cells and sip73*2. Columns, mean (n=3) ±SEM. E) Heat map representation of the most significantly up or downregulated genes after sip73*1. Genes involved in metabolism were plotted. Genes were identified using MSigDB and plotted to highlight differences in expression of 3 z-scores or greater between the two groups (red = relative upregulation, blue = relative downregulation). F) MB cells (DAOY, ICb-1299 and m137) were transiently transfected with scramble or sip73*1 for 10, 24 and 48h. Columns, mean (n=3) ±SEM; ***P<0.0001. G) DAOY cells were transiently transfected with scramble or sip73*1 human or sip73*1 human plus TAp73 mouse for 10 hours. RT-PCR was performed for TAp73 human, TAp73 mouse, GLS-2, ASL and GADD45B genes. Columns, mean (n=3) ±SEM; ***P<0.0001. H) DAOY cells were transfected with scramble or sip73*1. Western blot showing p73 and GLS-2 protein levels after silencing. GAPDH was used as a loading control.

Figure 2. p73KD induces mitochondrial defects and activates AMPK signalling. (A) DAOY cells were transfected with scramble, sip73 (sip73*1: 2671, sip73*2: 115666) or siGLS-2 (siGLS-2*1: s25941, siGLS-2*2: s223735). OCR in response to mitochondrial stress test were recorded to construct functional bioenergetic profiles. A minimum of five different samples were analysed for each group;***P<0.0001 (unpaired, two-sided t-test). A representative experimental data, out of three, is shown. B) Reduced and oxidized glutathione ratio was measured in DAOY cells after transient transfection with scramble, sip73*1, sip73*2, siGLS-2*1 and siGLS-2*2 for 24h. DAOY cells were infected with an empty vector or with shRNA (p73sKD*3 and p73sKD*5) alone or transfected with FLAG-GLS-2 expressing vector for 48h. (n=3). Data were mean ± SD. (*P < 0.01,**P<0.001,***P<0.0001). (C) DAOY cells were transfected with scramble or sip73 (sip73*1: 2671, sip73*2: 115666). ECAR was measured in response to mitochondrial stress test. A minimum of five different samples were analysed for each group;***P<0.0001 (unpaired, two-sided t-test). A representative experimental data, out of three, is shown. D-E) DAOY cells were transfected with scramble or sip73*2. After 8h of transfection the medium was changed and samples were collected after 6, 20, 30 and 40h. The results show glucose consumption (D) or lactate production (E). Columns, mean (n=4) ±SEM;**P<0.001,***P<0.0001. F) DAOY cells were transiently transfected with scramble, sip73*1 or sip73*2. After 48h, cells were collected and ATP levels were determined. Columns mean (n=4) ±SEM;***P<0.0001. G) DAOY cells were transfected with scramble or sip73*1 or sip73*2. After 48h a western blot was performed for ACC, P-ACC, S6K, P-S6K, eEF-2 and P-eEF-2. Intensity analysis is shown under each lane, scramble was considered 1. H) DAOY cells were transfected with scramble or sip73*1 or sip73*2. After 48h, cells were treated for 1h with puromycin 2.5mg/ml. Next, cells were collected and a western blot of lysed cells probed with a primary anti-puromycin antibody. Tubulin was used as a loading control. FCCP: Carbonyl cyanide-4-(trifluoromethoxy)phenylhydrazone. 2-DG: 2-Deoxy-D-glucose.

Figure 3. p73 regulates metabolic pathways in MB. DAOY cells were transfected with scramble or sip73*1 (ID: 2671). A) After 48h the medium was collected and amino acid levels were quantified (n=3). B) After 0, 24 and 48h cells were collected and RT-PCR was performed for TAp73α and PKM2 genes. Columns mean n=3; ±SEM,***P<0.0001. C-D) LC-HRMS metabolic profiling of DAOY scramble (●) and sip73*1 cells (▲). PCA score plots of the first two components, PC1 and PC2. The data were normalized to median fold change and pareto scale. C) Positive ionization mode (R2X=0.602 and Q2=0.137). D) Negative ionization mode (R2X=0.761 and Q2=0.355). E) List of the affected metabolites after p73KD in DAOY cells. [1]Confidently identified metabolites, identification was based on retention time, exact mass and fragmentation as compared to an analytical standard that was analyzed under the same conditions. [2]Putatively annotated metabolites, annotation was based on exact mass and fragmentation as compared to available reference spectra.

Figure 4. p73 is a marker of glutamine addiction in MB. A) DAOY and UW228-2 cells were cultured for 24h under normal medium, glucose (Glc starv), glutamine (Gln starv) and serine/glycine (Ser/Gly starv) starvation condition. DAOY and UW228-2 cells were collected and cell number were determined. (n=3); Data are represented as mean±SD.**P<0.001,***P<0.0001. B) Representative image of DAOY cells under normal medium, Glc starv, Gln starv and Ser/Gly starv for 15h. Cells were stained with the proliferation marker EdU (green) and nuclear marker DAPI (blue). C) Histogram shows mean fluorescence intensities of EdU in DAOY cells under normal medium, Glc starv, Gln starv and Ser/Gly starv for 15h.(n=300 cells), Data are represented

as mean±SD,***P<0.0001. D) DAOY and UW228-2 cells were cultured for 24h under normal medium, glucose (Glc starv), glutamine (Gln starv) and serine/glycine (Ser/Gly starv) starvation condition. DAOY and UW228-2 cells were collected and ATP levels were determined. (n=3); Data were mean±SD.**P<0.001,***P<0.0001. E) DAOY cells were cultured for 24h under normal medium, Glc starv, Gln starv and Ser/Gly starv. Next, cells were collected and a western blot of lysed cells was performed against p73. GAPDH was used as a loading control. F) DAOY cells were cultured for 20h under normal medium, Glc starv, Gln starv and Ser/Gly starv. Apoptosis was measured with Annexin V-FITC and PI for flow cytometry analysis. Images are representative of at least three independent experiments. G) DAOY, UW228-2 and ICb-1299 cells were cultured for 20h under normal medium, Gln starv and Gln starv plus 10μM MG132. Apoptosis was measured with Annexin V-FITC and PI for flow cytometry analyse, (n=3). Data are represented as mean±SD.**P<0.001,***P<0.0001.

Figure 5. Co-treatment of cisplatin plus glutamine starvation induces a synergic apoptotic effect in MB. A) DAOY cells were cultured for 18h under normal medium or Gln-starv with or without etoposide or cisplatin. Etoposide (+:6.8nM;++:13.6nM), cisplatin (+:16.6nM;++:33.3nM). Apoptosis was measured with Annexin V-FITC and PI for flow cytometry analysis.(n=3). Data are represented as mean±SD.**P<0.001,***P<0.0001. B) Histogram shows mean fluorescence intensities of EdU in ICb-1299 cells under control medium, Gln-starv or 4μM compound 968, with or without cisplatin 16.6nM for 18h. C-D) DAOY cells were infected with an empty vector or with shRNA p73sKD*3 and p73sKD*5. Cells were incubated for 36h under normal medium, Gln-starv or Gln-starv plus cisplatin 16.6nM. Apoptosis was measured with Annexin V-FITC and PI by flow cytometry (C) or ATP levels (D) (n=3). Data are represented as mean±SD.**P<0.001,***P<0.0001. E) Apoptosis was determined in DAOY, ICb-1299, m137 and UW228-2 cells. Cell were treated with cisplatin 16.6nM, Gln-starv, Gln-starv plus cisplatin 16.6nM DON 0.9mM or DON plus cisplatin 16.6nM. The cells were collected and stained with Annexin V-FITC and PI for flow cytometry analysis (n=3). Data were mean±SD. *P<0.01,***P<0.0001.

Figure 6. Glutamine starvation induces ROS and DNA damage in MB. A) DAOY and UW228-2 cells were cultured for 12h under normal medium, Glc starv, Gln starv and Ser/Gly starv. Cells were incubated with H_2DCFDA probe, an indicator for ROS. B) DAOY cells were cultured for 12h under normal medium, Gln starv or Gln starv plus 0.1 μM N-acetyl cysteine (NAC). Cells were incubated with H_2DCFDA and analysed by FACS. C-D) DAOY cells were cultured under normal medium, Glc starv, Gln starv or Ser/Gly starv for 20h. Also, DAOY cells were incubated with Glut starv plus cisplatin for 10h. C) Representative image of DAOY cells stained with the DNA damage marker γ-H_2AX (green) and nuclear marker DAPI (blue). Size bar=20μm. D) Histogram shows mean fluorescence intensities of EdU in DAOY cells (n=3), data are represented as mean±SD,***P<0.0001. E-F) DAOY and UW228-2 cells were cultured for 24h under normal medium, Glc starv, Gln starv or Ser/Gly starv. E) Reduced and oxidized glutathione ratio was measured by using the GSH/GSSG-Glo assay kit. F) Cells were collect and NADH absorbance was determined at 340nm by FACS analysis.

Figure 7. Glutamine restriction diet induces a significant improved survival in an orthotopic MB xenograft model. A-B) NOD-SCID mice were treated for 4 months with control diet or Gln-restriction diet. A) Glutamine, glutamate and serine levels were determined by ion-exchange chromatography in the cerebellum. B) Glutamine level was determined by ion-exchange chromatography in the CSF (n=5). Data are represented as mean±SD. **P<0.001,***P<0.0001**.** C-D) ICb-1299 human primary cells were injected in the cerebellum of new-born NOD-SCID mice and mice were divided into control diet (n=7), control diet + 2 doses cisplatin (n=11), control diet + 3 doses cisplatin (n=9), Gln-restriction diet (n=9), Gln-restriction diet + 2 doses cisplatin (n=8) or Gln-restriction diet + 3 doses cisplatin (n=7). C) Survival of mice is plotted over time, log-rank test. D) Histology of the MB tumors under control diet with 2 or 3 doses cisplatin or under Gln-restriction diet with 2 or 3 doses cisplatin, representative bright field images are shown for Ki-67 and cleaved caspase-3. Quantification is shown as mean of positive cells per high power field. Scale bar is 50μm.

References

Agostini M, Annicchiarico-Petruzzelli M, Melino G, Rufini A. 2016. Metabolic pathways regulated by TAp73 in response to oxidative stress. *Oncotarget* **7**: 29881-29900.

Ahluwalia GS, Grem JL, Hao Z, Cooney DA. 1990. Metabolism and action of amino acid analog anti-cancer agents. *Pharmacol Ther* **46**: 243-271.

Allocati N, Di Ilio C, De Laurenzi V. 2012. p63/p73 in the control of cell cycle and cell death. *Exp Cell Res* **318**: 1285-1290.

Altman BJ, Stine ZE, Dang CV. 2016. From Krebs to clinic: glutamine metabolism to cancer therapy. *Nat Rev Cancer*.

Amelio I, Cutruzzola F, Antonov A, Agostini M, Melino G. 2014a. Serine and glycine metabolism in cancer. *Trends Biochem Sci* **39**: 191-198.

Amelio I, Markert EK, Rufini A, Antonov AV, Sayan BS, Tucci P, Agostini M, Mineo TC, Levine AJ, Melino G. 2014b. p73 regulates serine biosynthesis in cancer. *Oncogene* **33**: 5039-5046.

Amores-Sanchez MI, Medina MA. 1999. Glutamine, as a precursor of glutathione, and oxidative stress. *Mol Genet Metab* **67**: 100-105.

Asher G, Tsvetkov P, Kahana C, Shaul Y. 2005. A mechanism of ubiquitin-independent proteasomal degradation of the tumor suppressors p53 and p73. *Genes Dev* **19**: 316-321.

Boominathan L. 2010. The guardians of the genome (p53, TA-p73, and TA-p63) are regulators of tumor suppressor miRNAs network. *Cancer Metastasis Rev* **29**: 613-639.

Buescher JM, Antoniewicz MR, Boros LG, Burgess SC, Brunengraber H, Clish CB, DeBerardinis RJ, Feron O, Frezza C, Ghesquiere B et al. 2015. A roadmap for interpreting (13)C metabolite labeling patterns from cells. *Curr Opin Biotechnol* **34**: 189-201.

Corno D, Pala M, Cominelli M, Cipelletti B, Leto K, Croci L, Barili V, Brandalise F, Melzi R, Di Gregorio A et al. 2012. Gene signatures associated with mouse postnatal hindbrain neural stem cells and medulloblastoma cancer stem cells identify novel molecular mediators and predict human medulloblastoma molecular classification. *Cancer Discov* **2**: 554-568.

DeBerardinis RJ, Cheng T. 2010. Q's next: the diverse functions of glutamine in metabolism, cell biology and cancer. *Oncogene* **29**: 313-324.

Dulloo I, Gopalan G, Melino G, Sabapathy K. 2010. The antiapoptotic DeltaNp73 is degraded in a c-Jun-dependent manner upon genotoxic stress through the antizyme-mediated pathway. *Proc Natl Acad Sci U S A* **107**: 4902-4907.

Evans AM, DeHaven CD, Barrett T, Mitchell M, Milgram E. 2009. Integrated, nontargeted ultrahigh performance liquid chromatography/electrospray ionization tandem mass spectrometry platform for the identification and relative quantification of the small-molecule complement of biological systems. *Anal Chem* **81**: 6656-6667.

Gershon TR, Crowther AJ, Tikunov A, Garcia I, Annis R, Yuan H, Miller CR, Macdonald J, Olson J, Deshmukh M. 2013. Hexokinase-2-mediated aerobic glycolysis is integral to cerebellar neurogenesis and pathogenesis of medulloblastoma. *Cancer Metab* **1**: 2.

Giovannini C, Matarrese P, Scazzocchio B, Sanchez M, Masella R, Malorni W. 2002. Mitochondria hyperpolarization is an early event in oxidized low-density lipoprotein-induced apoptosis in Caco-2 intestinal cells. *FEBS Lett* **523**: 200-206.

Haggblad Sahlberg S, Mortensen AC, Haglof J, Engskog MK, Arvidsson T, Pettersson C, Glimelius B, Stenerlow B, Nestor M. 2017. Different functions of AKT1 and AKT2 in molecular pathways, cell migration and metabolism in colon cancer cells. *Int J Oncol* **50**: 5-14.

Hanahan D, Weinberg RA. 2011. Hallmarks of cancer: the next generation. *Cell* **144**: 646-674.

Hardie DG, Ross FA, Hawley SA. 2012. AMPK: a nutrient and energy sensor that maintains energy homeostasis. *Nat Rev Mol Cell Biol* **13**: 251-262.

He Z, Liu H, Agostini M, Yousefi S, Perren A, Tschan MP, Mak TW, Melino G, Simon HU. 2013. p73 regulates autophagy and hepatocellular lipid metabolism through a transcriptional activation of the ATG5 gene. *Cell Death Differ* **20**: 1415-1424.

Hensley CT, Wasti AT, DeBerardinis RJ. 2013. Glutamine and cancer: cell biology, physiology, and clinical opportunities. *J Clin Invest* **123**: 3678-3684.

Hill RM, Kuijper S, Lindsey JC, Petrie K, Schwalbe EC, Barker K, Boult JK, Williamson D, Ahmad Z, Hallsworth A et al. 2015. Combined MYC and P53 defects emerge at medulloblastoma relapse and define rapidly progressive, therapeutically targetable disease. *Cancer Cell* **27**: 72-84.

Jiang P, Du W, Yang X. 2013. A critical role of glucose-6-phosphate dehydrogenase in TAp73-mediated cell proliferation. *Cell Cycle* **12**: 3720-3726.

Leprivier G, Remke M, Rotblat B, Dubuc A, Mateo AR, Kool M, Agnihotri S, El-Naggar A, Yu B, Somasekharan SP et al. 2013. The eEF2 kinase confers resistance to nutrient deprivation by blocking translation elongation. *Cell* **153**: 1064-1079.

Li ZQ, Gu XY, Hu JX, Ping Y, Li H, Yan JY, Li J, Sun R, Yu ZJ, Zhang Y. 2016. Hepatitis C virus core protein impairs metabolic disorder of liver cell via HOTAIR-Sirt1 signalling. *Biosci Rep* **36**.

Liu H, Zhang W, Wang K, Wang X, Yin F, Li C, Wang C, Zhao B, Zhong C, Zhang J et al. 2015. Methionine and cystine double deprivation stress suppresses glioma proliferation via inducing ROS/autophagy. *Toxicol Lett* **232**: 349-355.

Liu X, Yuan H, Niu Y, Niu W, Fu L. 2012. The role of AMPK/mTOR/S6K1 signaling axis in mediating the physiological process of exercise-induced insulin sensitization in skeletal muscle of C57BL/6 mice. *Biochim Biophys Acta* **1822**: 1716-1726.

Louis DN, Ohgaki H, Wiestler OD, Cavenee WK, Burger PC, Jouvet A, Scheithauer BW, Kleihues P. 2007. The 2007 WHO classification of tumours of the central nervous system. *Acta Neuropathol* **114**: 97-109.

Maddocks OD, Berkers CR, Mason SM, Zheng L, Blyth K, Gottlieb E, Vousden KH. 2013. Serine starvation induces stress and p53-dependent metabolic remodelling in cancer cells. *Nature* **493**: 542-546.

Maddocks OD, Labuschagne CF, Adams PD, Vousden KH. 2016. Serine Metabolism Supports the Methionine Cycle and DNA/RNA Methylation through De Novo ATP Synthesis in Cancer Cells. *Mol Cell* **61**: 210-221.

Mari M, Morales A, Colell A, Garcia-Ruiz C, Fernandez-Checa JC. 2009. Mitochondrial glutathione, a key survival antioxidant. *Antioxid Redox Signal* **11**: 2685-2700.

Marullo R, Werner E, Degtyareva N, Moore B, Altavilla G, Ramalingam SS, Doetsch PW. 2013. Cisplatin induces a mitochondrial-ROS response that contributes to cytotoxicity depending on mitochondrial redox status and bioenergetic functions. *PLoS One* **8**: e81162.

Meiser J, Tumanov S, Maddocks O, Labuschagne CF, Athineos D, Van Den Broek N, Mackay GM, Gottlieb E, Blyth K, Vousden K et al. 2016. Serine one-carbon catabolism with formate overflow. *Sci Adv* **2**: e1601273.

Mihaylova MM, Shaw RJ. 2011. The AMPK signalling pathway coordinates cell growth, autophagy and metabolism. *Nat Cell Biol* **13**: 1016-1023.

Moreno-Sanchez R, Rodriguez-Enriquez S, Saavedra E, Marin-Hernandez A, Gallardo-Perez JC. 2009. The bioenergetics of cancer: is glycolysis the main ATP supplier in all tumor cells? *Biofactors* **35**: 209-225.

Nicholson JK, Lindon JC, Holmes E. 1999. 'Metabonomics': understanding the metabolic responses of living systems to pathophysiological stimuli via multivariate statistical analysis of biological NMR spectroscopic data. *Xenobiotica* **29**: 1181-1189.

Niklison-Chirou MV, Steinert JR, Agostini M, Knight RA, Dinsdale D, Cattaneo A, Mak TW, Melino G. 2013. TAp73 knockout mice show morphological and functional nervous system defects associated with loss of p75 neurotrophin receptor. *Proc Natl Acad Sci U S A* **110**: 18952-18957.

Northcott PA Shih DJ Peacock J Garzia L Morrissy AS Zichner T Stutz AM Korshunov A Reimand J Schumacher SE et al. 2012. Subgroup-specific structural variation across 1,000 medulloblastoma genomes. *Nature* **488**: 49-56.

Phoenix TN, Patmore DM, Boop S, Boulos N, Jacus MO, Patel YT, Roussel MF, Finkelstein D, Goumnerova L, Perreault S et al. 2016. Medulloblastoma Genotype Dictates Blood Brain Barrier Phenotype. *Cancer Cell* **29**: 508-522.

Pozniak CD, Barnabe-Heider F, Rymar VV, Lee AF, Sadikot AF, Miller FD. 2002. p73 is required for survival and maintenance of CNS neurons. *J Neurosci* **22**: 9800-9809.

Ramaswamy V, Nor C, Taylor MD. 2015. p53 and Meduloblastoma. *Cold Spring Harb Perspect Med* **6**: a026278.

Rosenbluth JM, Pietenpol JA. 2009. mTOR regulates autophagy-associated genes downstream of p73. *Autophagy* **5**: 114-116.

Rufini A, Niklison-Chirou MV, Inoue S, Tomasini R, Harris IS, Marino A, Federici M, Dinsdale D, Knight RA, Melino G et al. 2012. TAp73 depletion accelerates aging through metabolic dysregulation. *Genes Dev* **26**: 2009-2014.

Talos F, Abraham A, Vaseva AV, Holembowski L, Tsirka SE, Scheel A, Bode D, Dobbelstein M, Bruck W, Moll UM. 2010. p73 is an essential regulator of neural stem cell maintenance in embryonal and adult CNS neurogenesis. *Cell Death Differ* **17**: 1816-1829.

Taylor MD, Northcott PA, Korshunov A, Remke M, Cho YJ, Clifford SC, Eberhart CG, Parsons DW, Rutkowski S, Gajjar A et al. 2012. Molecular subgroups of medulloblastoma: the current consensus. *Acta Neuropathol* **123**: 465-472.

Tech K, Deshmukh M, Gershon TR. 2015. Adaptations of energy metabolism during cerebellar neurogenesis are co-opted in medulloblastoma. *Cancer Lett* **356**: 268-272.

Vanbokhoven H, Melino G, Candi E, Declercq W. 2011. p63, a story of mice and men. *J Invest Dermatol* **131**: 1196-1207.

Velletri T, Romeo F, Tucci P, Peschiaroli A, Annicchiarico-Petruzzelli M, Niklison-Chirou MV, Amelio I, Knight RA, Mak TW, Melino G et al. 2013. GLS2 is transcriptionally regulated by p73 and contributes to neuronal differentiation. *Cell Cycle* **12**: 3564-3573.

Warburg O. 1956. On the origin of cancer cells. *Science* **123**: 309-314.

Wise DR, Thompson CB. 2010. Glutamine addiction: a new therapeutic target in cancer. *Trends Biochem Sci* **35**: 427-433.

Wu CA, Chao Y, Shiah SG, Lin WW. 2013. Nutrient deprivation induces the Warburg effect through ROS/AMPK-dependent activation of pyruvate dehydrogenase kinase. *Biochim Biophys Acta* **1833**: 1147-1156.

Yang A, Walker N, Bronson R, Kaghad M, Oosterwegel M, Bonnin J, Vagner C, Bonnet H, Dikkes P, Sharpe A et al. 2000. p73-deficient mice have neurological, pheromonal and inflammatory defects but lack spontaneous tumours. *Nature* **404**: 99-103.

Zhao J, Zhai B, Gygi SP, Goldberg AL. 2015. mTOR inhibition activates overall protein degradation by the ubiquitin proteasome system as well as by autophagy. *Proc Natl Acad Sci U S A* **112**: 15790-15797.

Zhu J, Jiang J, Zhou W, Chen X. 1998. The potential tumor suppressor p73 differentially regulates cellular p53 target genes. *Cancer Res* **58**: 5061-5065.

Zitterbart K, Zavrelova I, Kadlecova J, Spesna R, Kratochvilova A, Pavelka Z, Sterba J. 2007. p73 expression in medulloblastoma: TAp73/DeltaNp73 transcript detection and possible association of p73alpha/DeltaNp73 immunoreactivity with survival. *Acta Neuropathol* **114**: 641-650.

NiklisonChirou_Fig1

A

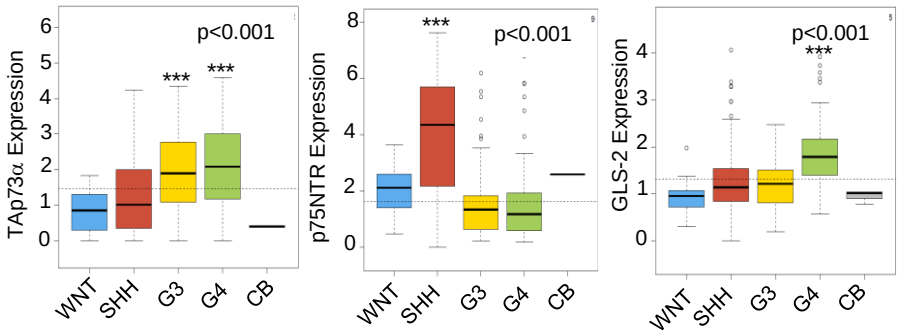

B

		Cell number/ml	% of growth	Apoptosis (SubG1 % cells)
DAOY	control	$9.22 \pm 0.9\ 10^4$	100	1.05
	sip73*1	$5.87 \pm 0.6\ 10^4$	63.66	1.1
	sip73*2	$3.91 \pm 0.7\ 10^4$	42.4	1.4
m137	control	$1.14 \pm 0.2\ 10^6$	100	1
	sip73*2	$0.55 \pm 0.4\ 10^6$	48.24	1.2
ICb-1299	control	$1.32 \pm 0.2\ 10^6$	100	1
	sip73*2	$0.85 \pm 0.4\ 10^6$	64.39	1.1

C

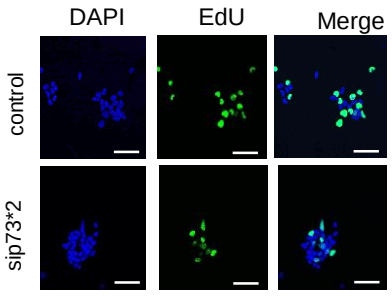

D

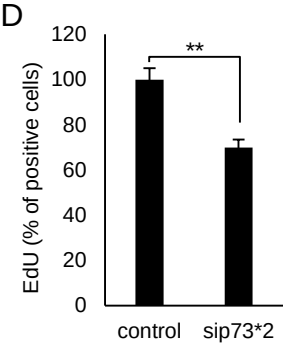

E

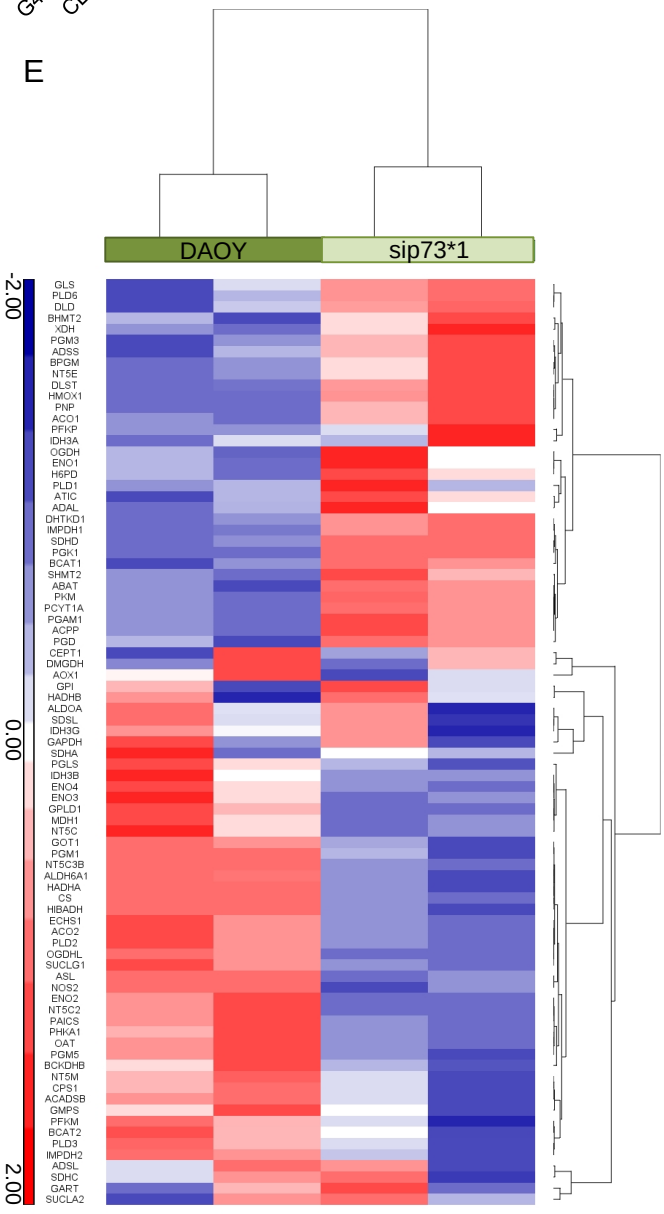

F

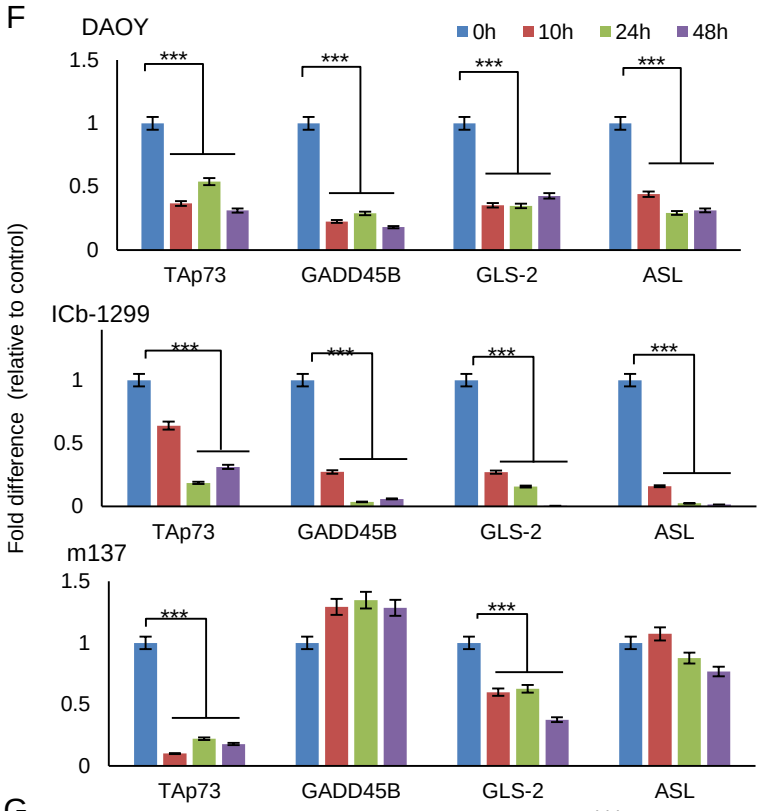

G

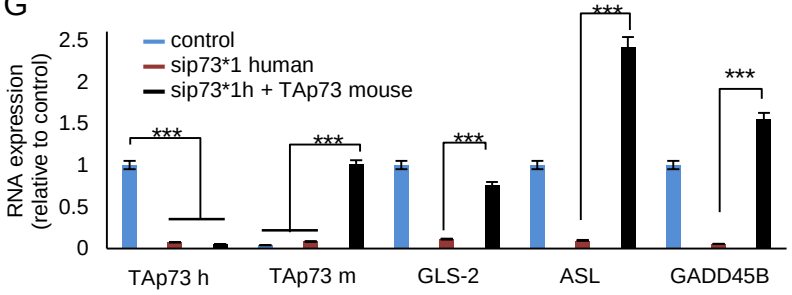

H

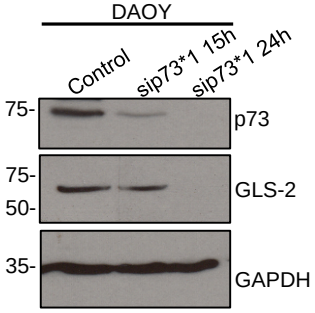

NiklisonChirou_Fig2

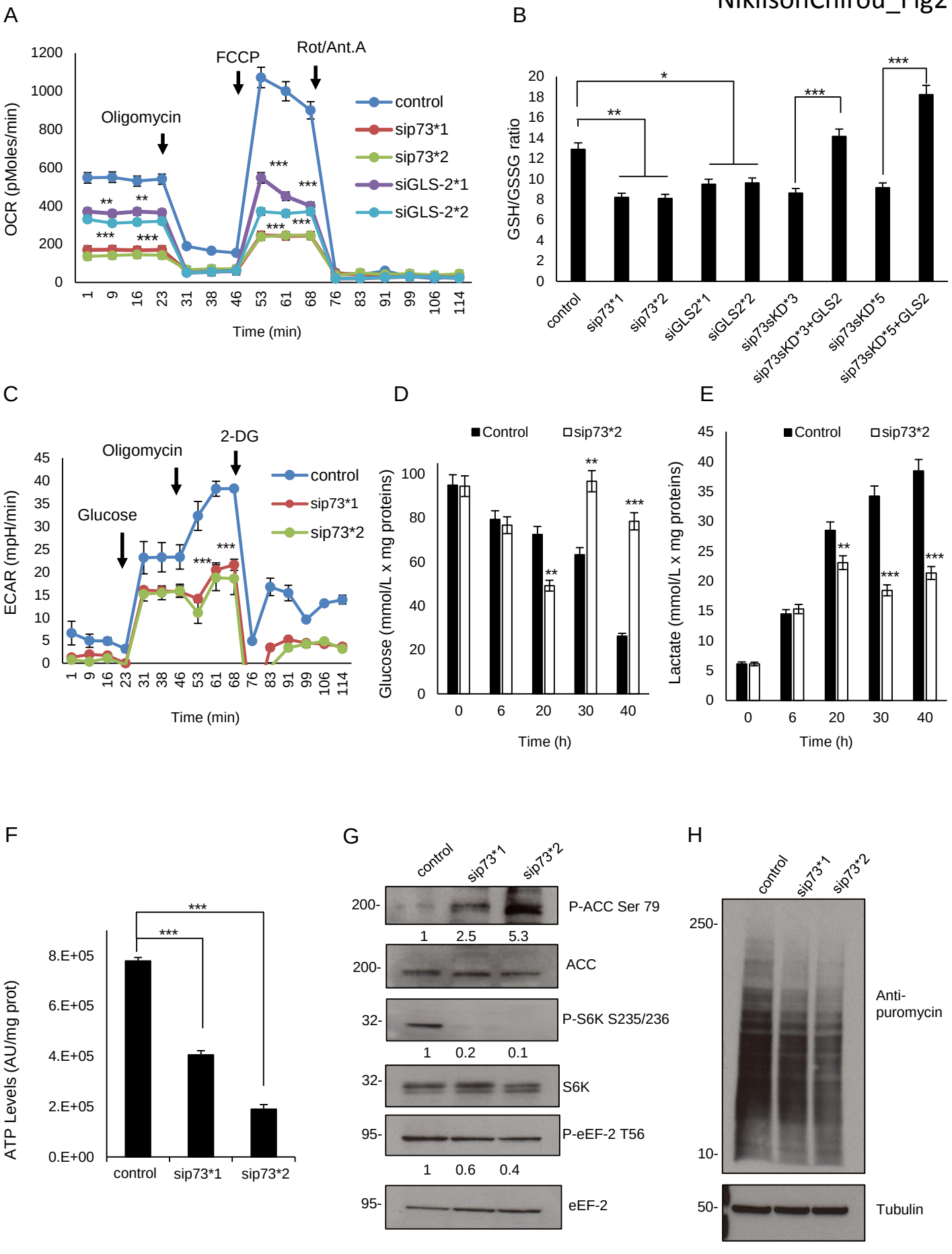

NiklisonChirou_Fig3

A

Amino acid concentration (mmol/L.mg of proteins)	Control	sip73*1
Serine	1163.4 ± 25	5465.1 ± 32
Glycine	1450.5± 54	3237.2 ± 73
Ornithine	173.3 ± 20	590.7 ± 12
Proline	113.9 ± 21	163.2 ± 4
Glutamate	1391.1 ± 64	116.3 ± 8
Glutamine	2985.1 ± 42	0.0 ± 0
Arginine	1133.7 ± 36	779.0 ± 8
Taurine	29.7 ± 5	5.0 ± 0
Alanine	6242.6 ± 47	76.5 ± 6
Valine	2742.6 ± 96	1255.8 ± 78
Methionine	579.2 ± 18	279.1 ± 67
Isoleucine	2386.1 ± 36	1097.7 ± 45
Leucine	2495.1 ± 12	1190.7 ± 34
Tyrosine	1331.7 ± 66	632.6 ± 82
Phenylalanine	1381.2 ± 53	637.2 ± 35
Lysine	2683.2 ± 69	1255.8 ± 29
Threonine	2747.5 ± 33	1283.7 ± 26
Citrulline	54.5 ± 3	50.0 ± 0
Histidine	668.3 ± 45	623.3 ± 23

B

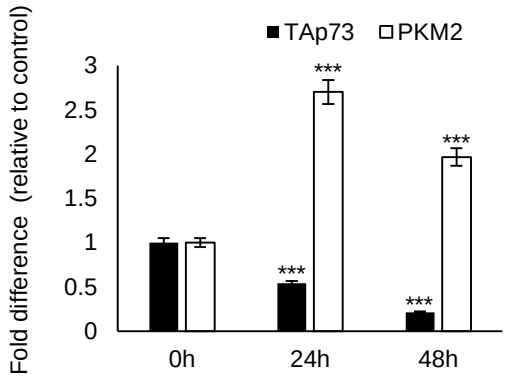

C

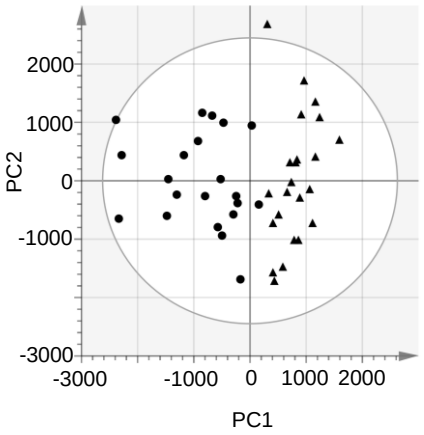

D

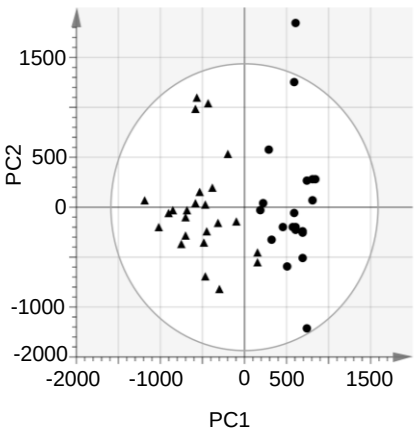

E

Metabolite	Fold change	p-value	Experimental m/z	Substance class
Adenosine [2]	-1,18 ± 0,18	0,0491	$[M-H]^-$ 266.0868 $[M+Cl]^-$ 302.0634	Nucleoside
Cytidine [1]	2,08 ± 0,63	0,0002	$[M+Na]^+$ 266.0747 $[M+K]^+$ 282.0489 $[F+H]^+$ 112.0505 $[F+Na]^+$ 134.0328 $[M-H]^-$ 242.0758	Nucleoside
Guanine [2]	4,04 ± 0,73	7.35×10^{-6}	$[M+H]^+$ 152.0582 $[M-H]^-$ 150.0393	Purine
Guanosine [2]	2,13 ± 0,61	$1,716\times10^{-5}$	$[M-H]^-$ 282.0817	Nucleoside
Hypoxanthine [1]	1,52 ± 0,17	$9,956\times10^{-10}$	$[M+Na]^+$ 159.0280 $[M+2Na-H]^+$ 181.0099	Purine
Inosine [2]	2,13 ± 0,41	$1,121\times10^{-9}$	$[F+H]^+$ 137.0613 $[M-H]^-$ 267.2067	Nucleoside
Uridine [1]	1,58 ± 0,39	0,0012	$[M-H]^-$ 279.0372 $[F]^-$ 110.0218 $[F]^-$ 152.0320	Nucleoside
5´-methylthioadenosine [2]	2,40 ± 0,32	$1,638\times10^{-16}$	$[M+H]^+$ 298.0974	Nucleoside derivative
Choline [1]	-1,82 ± 0,17	$1,514\times10^{-13}$	$[M+H]^+$ 104.1073	Choline
Phenylalanine [1]	1,52 ± 0,41	0,0063	$[M-H]^-$ 164.0688	Amino acid
Indoleacetic acid [2]	2,03 ± 0,30	$3,335\times10^{-11}$	$[M-H_2O+H]^+$ 176.0712	Organic acid
N-Formyl-L-Methionine [2]	2,66 ± 0,88	0,0001	$[M-H_2O+H]^+$ 160.0432	Methionine derivative
4-phosphopantothenoylcysteine [2]	1,76 ± 0,45	0,0001	$[M-H]^-$ 401.0796	Organic acid
Pyruvic acid [1]	1,99 ± 0,70	0,0014	$[M+FA-H]^-$ 133.0128	Organic acid
Malic acid [1]	-1,15 ± 0,11	0,0006	$[M-H_2O-H]^-$ 114.9856	Organic acid

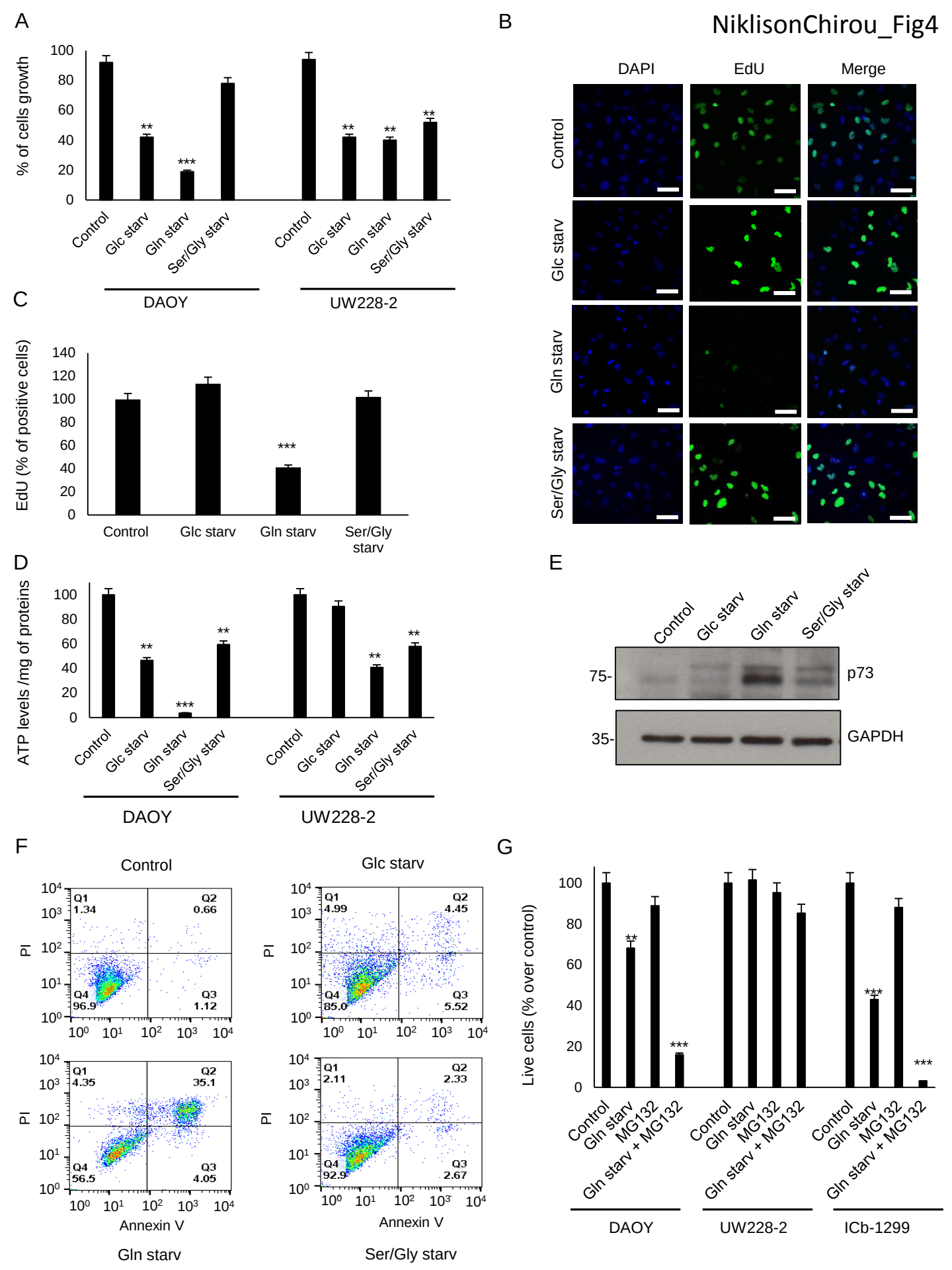
NiklisonChirou_Fig4
A
% of cells growth
Control
Glc starv
Gln starv
Ser/Gly starv
DAOY
UW228-2
B
DAPI
EdU
Merge
C
EdU (% of positive cells)
D
ATP levels /mg of proteins
E
75-
p73
35-
GAPDH
F
Control
Glc starv
Gln starv
Ser/Gly starv
PI
Annexin V
Q1
Q2
Q3
Q4
G
Live cells (% over control)
MG132
Gln starv + MG132
ICb-1299

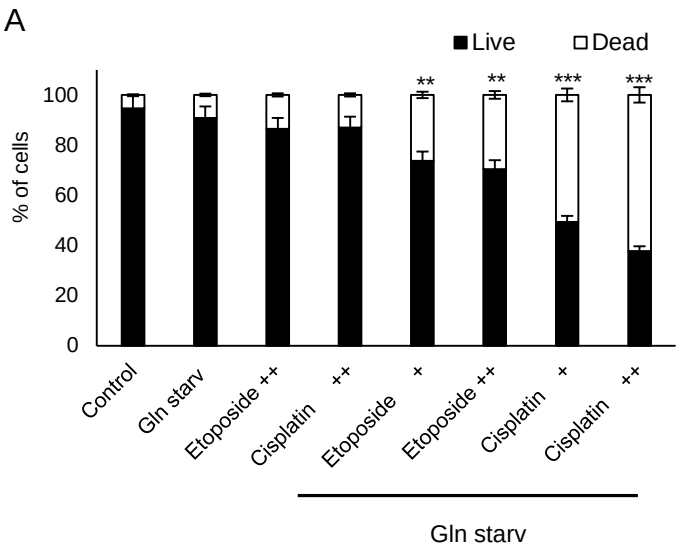
A
Live
Dead
% of cells
100
80
60
40
20
0
**
**
***
***
Control
Gln starv
Etoposide ++
Cisplatin ++
Etoposide +
Etoposide ++
Cisplatin +
Cisplatin ++
Gln starv

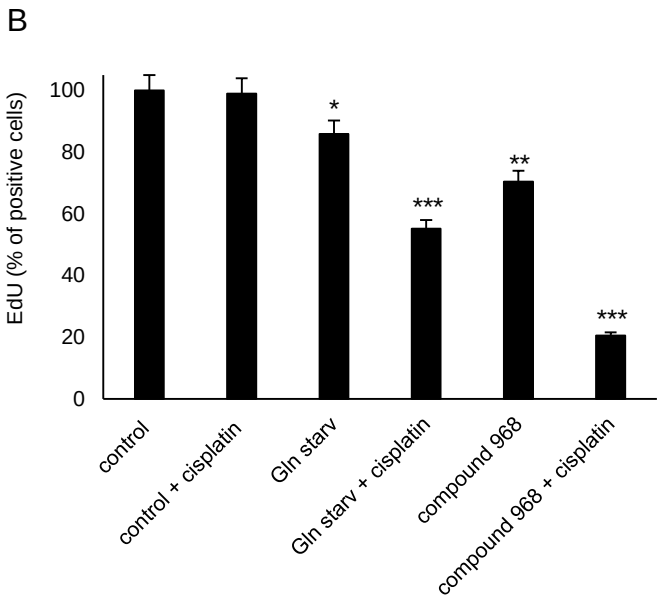
B
EdU (% of positive cells)
100
80
60
40
20
0
*
***
**
***
control
control + cisplatin
Gln starv
Gln starv + cisplatin
compound 968
compound 968 + cisplatin

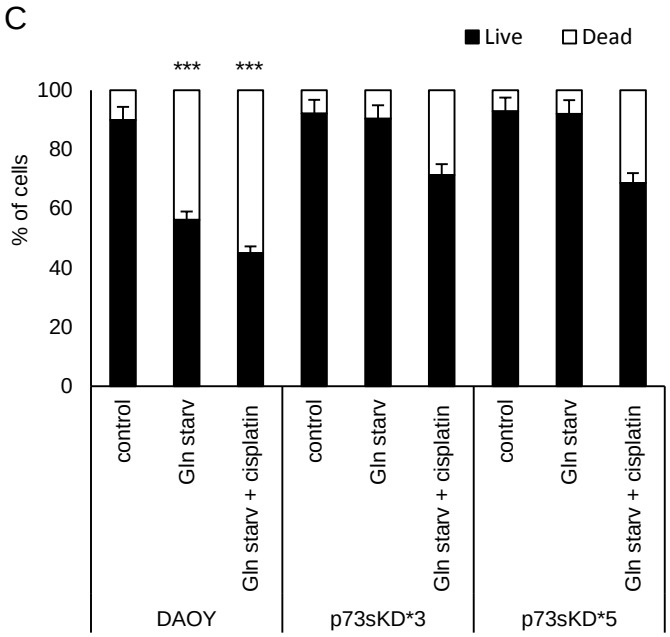
C
Live
Dead
% of cells
100
80
60
40
20
0
***
***
control
Gln starv
Gln starv + cisplatin
DAOY
p73sKD*3
p73sKD*5

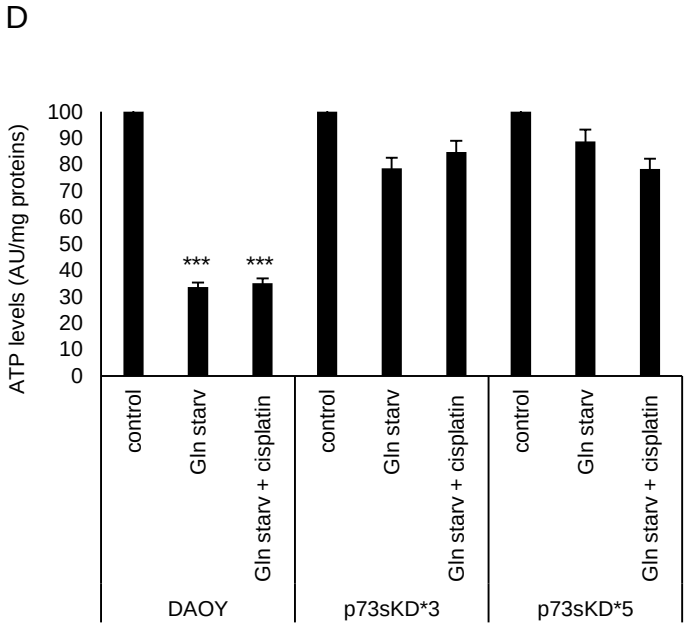
D
ATP levels (AU/mg proteins)
100
90
80
70
60
50
40
30
20
10
0
***
***
control
Gln starv
Gln starv + cisplatin
DAOY
p73sKD*3
p73sKD*5

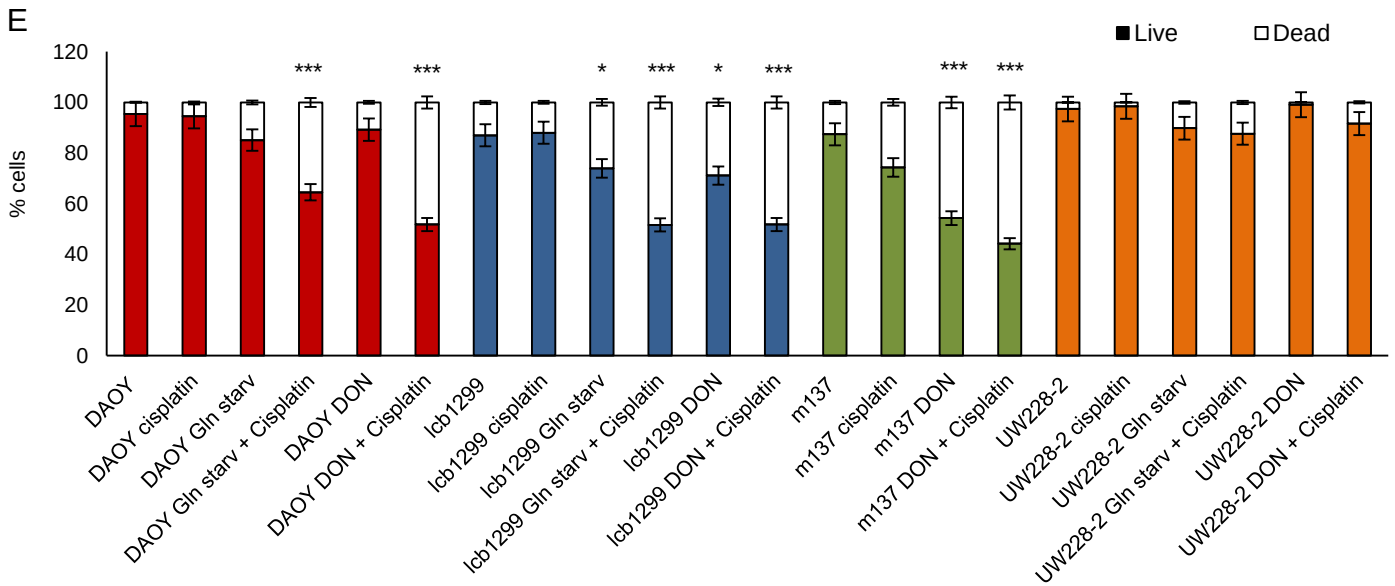
E
Live
Dead
% cells
120
100
80
60
40
20
0
***
***
*
***
*
***
***
***
DAOY
DAOY cisplatin
DAOY Gln starv
DAOY Gln starv + Cisplatin
DAOY DON
DAOY DON + Cisplatin
Icb1299
Icb1299 cisplatin
Icb1299 Gln starv
Icb1299 Gln starv + Cisplatin
Icb1299 DON
Icb1299 DON + Cisplatin
m137
m137 cisplatin
m137 DON
m137 DON + Cisplatin
UW228-2
UW228-2 cisplatin
UW228-2 Gln starv
UW228-2 Gln starv + Cisplatin
UW228-2 DON
UW228-2 DON + Cisplatin

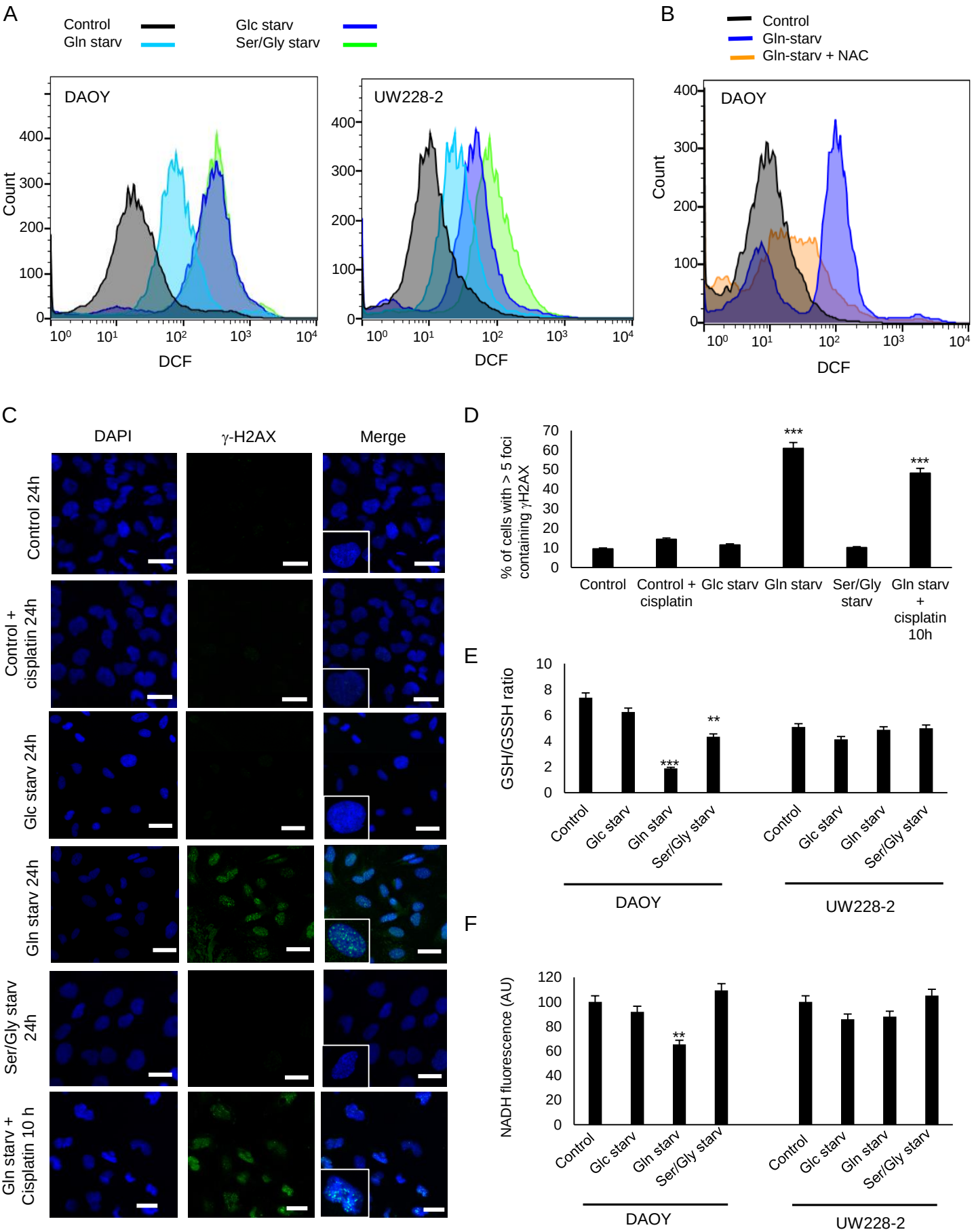
A
Control
Gln starv
Glc starv
Ser/Gly starv
DAOY
UW228-2
Count
DCF
B
Control
Gln-starv
Gln-starv + NAC
DAOY
Count
DCF
C
DAPI
γ-H2AX
Merge
Control 24h
Control + cisplatin 24h
Glc starv 24h
Gln starv 24h
Ser/Gly starv 24h
Gln starv + Cisplatin 10 h
D
% of cells with > 5 foci containing γH2AX
Control
Control + cisplatin
Glc starv
Gln starv
Ser/Gly starv
Gln starv + cisplatin 10h
E
GSH/GSSH ratio
Control
Glc starv
Gln starv
Ser/Gly starv
DAOY
UW228-2
F
NADH fluorescence (AU)
Control
Glc starv
Gln starv
Ser/Gly starv
DAOY
UW228-2

A

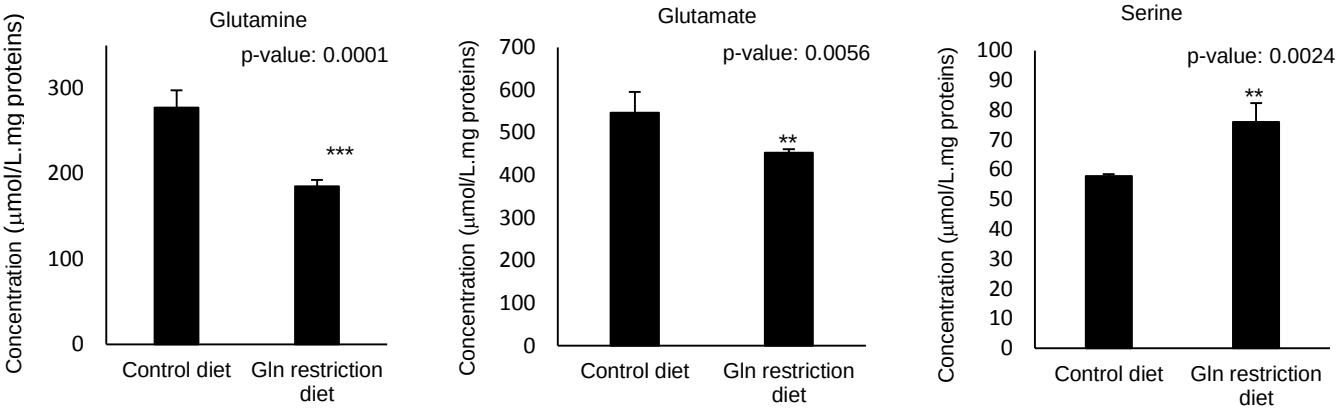

B

C

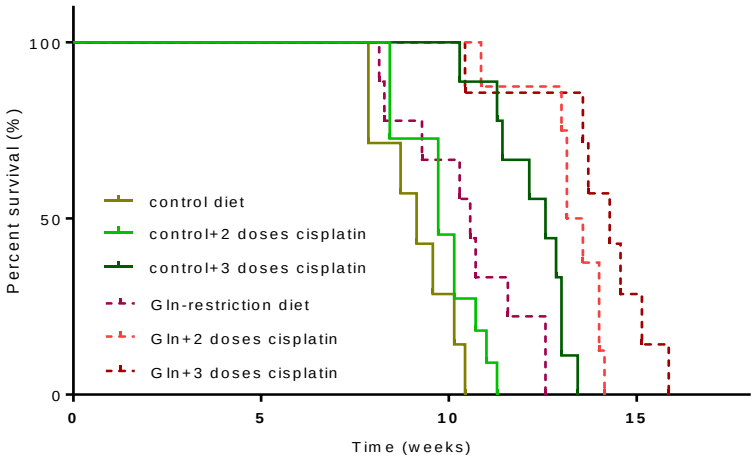

	P value	P value summary
Control diet vs Gln-restriction diet	0.024	*
Control+2 doses cisplatin vs Gln+2 doses cisplatin	<0.0001	****
Control+3 doses cisplatin vs Gln+3 doses cisplatin	0.002	**

D